JVST A
Journal of Vacuum Science & Technology A

Phase-separated indenofluorene arrays stabilized by hydrogen and halogen bonds on Au(111)

Cite as: J. Vac. Sci. Technol. A **40**, 013201 (2022); https://doi.org/10.1116/6.0001345
Submitted: 09 August 2021 • Accepted: 05 November 2021 • Published Online: 29 November 2021

Jong Hwan Park, Min Hui Chang, Won Jun Jang, et al.

JVST A
Journal of Vacuum Science & Technology A

ARTICLE

avs.scitation.org/journal/jva

Phase-separated indenofluorene arrays stabilized by hydrogen and halogen bonds on Au(111)

Cite as: J. Vac. Sci. Technol. A 40, 013201 (2022); doi: 10.1116/6.0001345
Submitted: 9 August 2021 · Accepted: 5 November 2021 ·
Published Online: 29 November 2021

Jong Hwan Park,[1] Min Hui Chang,[1] Won Jun Jang,[2] Seungwu Han,[3] and Se-Jong Kahng[1,a)]

AFFILIATIONS

[1]Department of Physics, Korea University, 145 Anam-ro, Seongbuk-gu, Seoul 02841, Republic of Korea
[2]Samsung Advanced Institute of Technology, Samsung Electronics, Suwon, Gyeonggi-do 16678, Republic of Korea
[3]Department of Materials Science and Engineering, Seoul National University, 1 Gwanak-ro, Gwanak-gu, Seoul 08826, Republic of Korea

[a)]**Author to whom correspondence should be addressed:** sjkahng@korea.ac.kr

ABSTRACT

Indenofluorene, which consists of a 6-5-6-5-6 fused-ring structure, is a semiconducting molecule with possible applications in optoelectronic devices. Bulk crystal structures, molecular front orbitals, and on-surface polymerized indenofluorene have recently been studied, but self-assembled structures on the surface have not yet been reported. Here, we report the array structure of 2,8-dibromoindeno[1,2-b]fluorene-6,12-dione on Au(111) studied using scanning tunneling microscopy. We proposed an alternating-tread stair structure as the molecular model for the monolayer molecular islands, which show strong shape anisotropy. The model can be explained by four O···H hydrogen bonds and one Br···Br halogen bond per molecule, as supported by density functional theory calculations. Although they prefer intermixed heteroprochiral structures in bulk layers, our study shows that these molecules can form phase-separated homoprochiral structures on the surface, leading to potential applications in molecular chiral separation.

I. INTRODUCTION

Small molecules with many π-electrons can form crystals and films with an energy bandgap, making them suitable for use in electronic devices, with additional advantages of facile fabrication, mechanical flexibility, and a low cost.[1–6] Indenofluorene, which consists of a 6-5-6-5-6 fused-ring structure, is an example of one of these molecules that has received significant research attention in recent years. It has 20 π-electrons per molecule that are fully conjugated in a planar configuration, leading to typical n-type semiconducting behavior.[7–10] Because of its unique optical properties, it can be potentially employed in organic light-emitting diodes and organic light-emitting transistors.[11–13] The crystal structure of indenofluorene has been studied with x-ray diffraction and density functional theory (DFT) calculations, showing stacking layers of two-dimensional (2D) networks.[14,15] In each layer, fused rings and end groups lie in a plane with negligible interplanar twists. The molecules form strong intermolecular bonds within the same plane, exhibiting continuous graphene-like 2D networks that are effective for electron conduction. On metal surfaces, front-orbital structures of adsorbed single indenofluorene molecules have been visualized, and the *on-surface* synthesis of polymeric indenofluorene chains has been actively studied using scanning tunneling microscopy (STM).[16–20] However, the self-assembly of indenofluorene structures on metal surfaces has not yet been reported in the literature.

In the present study, we investigated the array structure of 2,8-dibromoindeno[1,2-b]fluorene-6,12-dione (DBIFD) on Au (111) using STM. We observed an alternating-tread stair structure in the monolayer molecular islands that demonstrated strong anisotropy and proposed an atomistic model that can be explained using O···H and Br···Br halogen bonds, as supported by DFT calculations. Our study revealed that the observed structures were phase-separated homoprochiral domains that are in striking contrast to previously reported intermixed heteroprochiral structures in bulk molecular layers.

II. EXPERIMENTAL METHODS

Experiments were conducted using a home-built STM system housed in an ultrahigh vacuum chamber with a base pressure below 1×10^{-10} Torr. The Au(111) surface was prepared from an

Au thin film (200 nm thick) on mica that was exposed to several cycles of Ne-ion sputtering and annealing at 800 K over the course of 1 h. The cleanliness of the Au(111) surface was confirmed by the presence of a typical herringbone structure on the terraces in the STM images. Commercial DBIFD (Tokyo Chemical Industry, Japan) was thermally evaporated from an alumina-coated crucible onto the surface to provide submonolayer coverage while maintaining the substrate temperature at about 150 K. The molecular source was outgassed for several hours prior to deposition. The prepared sample was transferred to the STM system, and measurements were conducted at 80 K using a Pt-Rh alloy tip.

III. THEORETICAL CALCULATIONS

DFT calculations were performed using the VASP code.[21,22] The interaction between ions and electrons was approximated using the projector-augmented wave method.[23] Generalized gradient approximation with the Perdew–Burke–Ernzerhof functional was used to determine the exchange-correlation energies between the electrons.[24] The energy cutoff for the plane-wave basis was set at 500 eV. To include nonbonding interactions between the molecules, especially van der Waals interactions, the dispersion-corrected DFT-D2 functional was adopted.[25,26] A unit cell containing a DBIFD molecule was used to form the periodic structure. The height of the simulation cell perpendicular to the molecular plane was fixed at 30 Å, while the lateral cell parameters (a, b) were optimized to ensure that the residual stress was under 6.2 meV/Å^3.

IV. RESULTS AND DISCUSSION

Figure 1(a) presents a ball-and-stick model of a DBIFD molecule, showing an alternating series of three hexagon and two pentagon rings with eight H atoms, two O atoms on the sides, and two Br atoms at the ends, which can possibly form hydrogen and halogen bonds. When the molecules were deposited at about 150 K, they formed molecular islands with no particular molecular order, but after annealing at temperatures higher than 200 K, molecular islands with strong anisotropy and directionality appeared. The aspect ratio of these molecular islands was higher than 8:1 [Figs. 1(b) and 1(c)]. The long edge of the molecular islands was aligned with [11$\bar{2}$] along the direction of the herringbone reconstructions of Au(111). Figures 2(a)–2(d) display higher-resolution STM images of the molecular islands. A single DBIFD molecule is represented as a bar with two bright balls corresponding to Br atoms at both ends. In Figs. 2(b) and 2(d), a molecular model overlays the STM images. The model has an alternating-tread stair structure, with each DBIFD molecule acting as an individual tread.

To explain the molecular model derived from our experiments, we calculated the intramolecular electrostatic potential distribution for an isolated molecule using DFT. Figure 3(a) shows an electrostatic potential of 0.02 e/Å mapped on an isosurface.[3] While the H and O atoms exhibit positive and negative electronic potentials, respectively, the Br atoms show a unique structure with σ-holes exhibiting both positive and negative electronic potentials in an atomic sphere.[27–44] Based on the potential distribution of individual DBIFD molecules, we constructed a simplified form of the electrostatic potential distribution around the Br, O, and H atoms and then superimposed this onto the experimental model as shown in Fig. 3(b). We were able to deduce the possible interactions between adjacent molecules; the cyan and red dotted lines represent possible O···H hydrogen bonds and Br···Br halogen bonds, respectively.[33–37](Colored figures are available online.)

To understand the precise arrangement of the DBIFD molecules, we performed DFT calculations for the molecular lattice structure. In these calculations, we considered free molecules. It has been reported that planar organic molecules have numerous adsorption sites on metal surfaces. In particular, for Au(111), the variation in adsorption energy is relatively modest considering the energy gains from the intermolecular interactions.[45] A clearer understanding would be possible by including the substrate. A parallelogram unit cell was adopted to construct the periodic structure

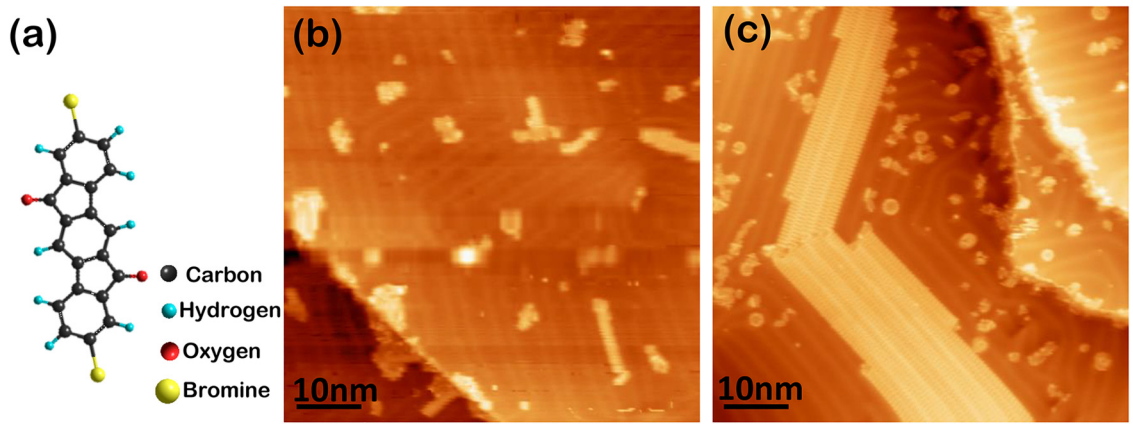

FIG. 1. (a) Ball-and-stick model of a 2,8-dibromoindeno[1,2-b]fluorene-6,12-dione (DBIFD) molecule. (b) and (c) Typical STM images (64 × 64 nm^2) of DBIFD molecules on the Au(111) surface after annealing at (b) 200 K (0.1 ML) and (c) 300 K (0.3 ML). Tunneling current: (b) I_T = 0.1 nA and (c) I_T = 0.05 nA. Sample voltage: (b) V_S = 1.1 V and (c) V_S = −1.6 V.

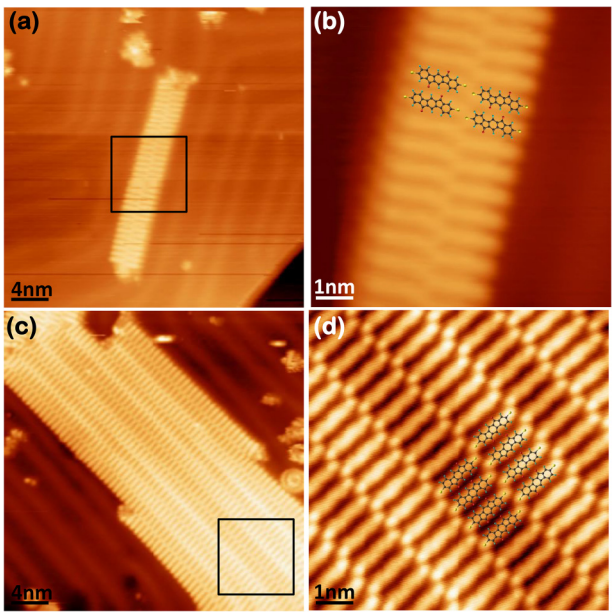

FIG. 2. (a)–(d) High-resolution STM images of 2D DBIFD structures. STM images in (b) and (d) are magnified from the squared regions in (a) and (c), respectively. Molecular models of DBIFD are superimposed over the STM images. The sizes of the STM images: (a) and (c) $32 \times 32\ nm^2$; (b) and (d) $8 \times 8\ nm^2$. Tunneling current: (a) and (b) $I_T = 0.1$ nA; (c) and (d) $I_T = 0.05$ nA. Sample voltage: (a) $V_S = -1.2$ V, (b) $V_S = -0.4$ V, (c) $V_S = -1.0$ V, and (d) $V_S = 0.6$ V.

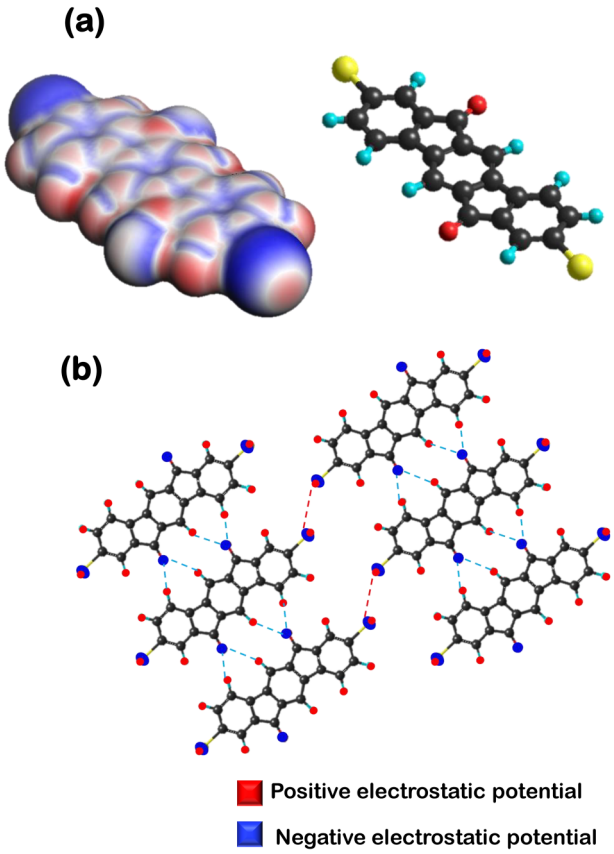

FIG. 3. (a) Calculated electrostatic potential distribution (isodensity surface plot) of a DBIFD molecule. (b) Schematic illustration of the intermolecular interactions between neighboring molecules with a simplified electrostatic potential distribution around the Br, O, and H atoms. The positive and negative potentials are colored red and blue, respectively. The dashed red and blue lines represent possible hydrogen and halogen bonds, respectively. (Color online.)

[Fig. 4(a)]. We considered the side lengths (a, b) of the parallelogram to be two independent parameters with an angle of 77° estimated from the experimental model. We performed calculations for various sets of (a, b), and obtained binding energies in the range of 200–600 meV per molecule [Fig. 4(b)]. The most stable structure was found at $a = 0.73$ nm and $b = 1.72$ nm, in reasonable agreement with the experimental observations ($a = 0.73$ nm and $b = 1.74$ nm). The largest energy gain was 540 meV per molecule, representing an average intermolecular bond of 108 meV. We extracted the lengths of the possible intermolecular bonds from a relaxed geometry. The computational results produced lengths of 0.22 and 0.25 nm for the O···H hydrogen bonds, depicted by the cyan and gray dotted lines in Fig. 4(a), respectively, and a length of 0.38 nm for the Br···Br halogen bond. The sums of the van der Waals radii are 0.27 nm for O···H hydrogen bonds and 0.37 nm for Br···Br halogen bonds. When the distance between two atoms is smaller than or similar to the sum of van der Waals radii of them, it is often considered that the two atoms form intermolecular bonds. Typical bond lengths for O···H and Br···Br are 0.18–0.26 and 0.32–0.42 nm, respectively.[46,47] The molecular structure had four O···H hydrogen bonds and one Br···Br halogen bond per molecule along the direction of lattice vectors **a** and **b**, respectively, which explains the observed anisotropy in the molecular islands. When a new molecule joins an existing molecular island, the formation of four O···H hydrogen bonds is always preferred to the formation of one Br···Br halogen bond. That is because typical binding energy of an O···H hydrogen bond is in the similar range to that of a Br···Br halogen bond.[28–31] The observed aspect ratio of the molecular islands roughly corresponded to the ratio of binding energies for two different sites on the long and short sides of the islands. Although the number of intermolecular bonds had a ratio of 4:1, the observed anisotropy in the island shapes had a ratio higher than 8:1, which indicates that the average binding energy of an O···H hydrogen bond must be at least twice as large as that of a Br···Br halogen bond. Molecular diffusivity can allow another scenario for islands anisotropy. Because of the herringbone reconstructions, it is easy for molecules to move along $[11\bar{2}]$ but hard to move along $1\bar{1}0$. The high aspect ratios in molecular islands can be induced by this diffusion anisotropy.

DBIFD molecules do not exhibit chirality in gas and liquid phases. However, when they are adsorbed onto the surface, they become chiral, which is known as prochirality. This is because flipping an adsorbed molecule requires a considerable amount of

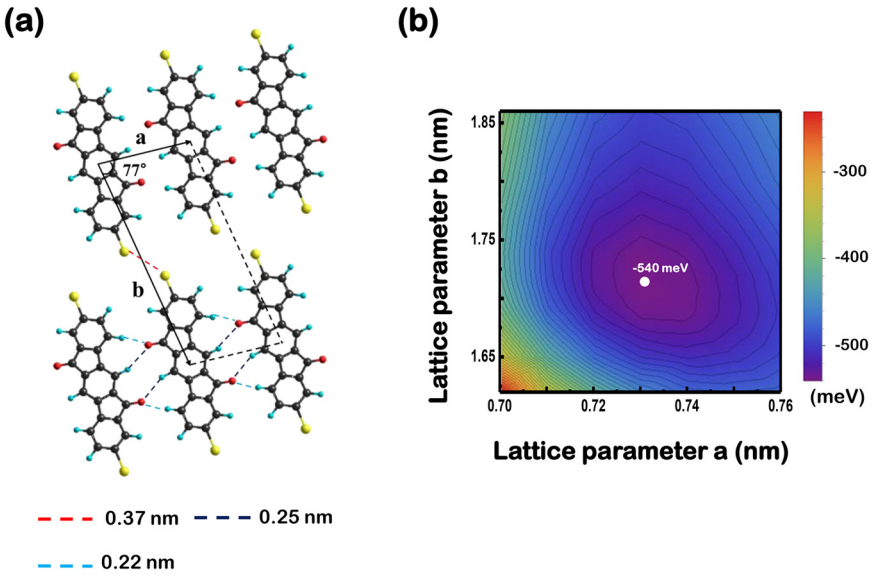

FIG. 4. (a) Calculated results for the relaxed 2D structure of DBIFD molecules from DFT calculations. (b) Energy gains per molecule as a function of lattice parameters (*a, b*) for 2D structures with an angle of 77°.

excitation energy. The molecular structures considered to this point in this article consisted of single-type prochiral molecules (δ-DBIFD). Nevertheless, we also observed a molecular structure comprising different-type prochiral molecules (λ-DBIFD), as shown in Figs. 5(a) and 5(b). Thus, the observed DBIFD structures were phase-separated and homoprochiral. Although the number of islands we considered was not enough for the statistical analysis, roughly half of them (54%) were δ-phase domains. Previous x-ray diffraction and DFT calculations performed on bulk crystals have revealed that DBIFD molecules form stacking layers of 2D structures, and each molecular layer has an intermixed heteroprochiral structure in which δ and λ-DBIFD rows alternate, which contrasts with our phase-separated structure on Au(111).[14,15] The intermixed structure has two O···H and two Br···H hydrogen bonds per molecule with distances of 0.27 and 0.31 nm, respectively. Thus, the phase-separated structure has one additional intermolecular bond per molecule and a much shorter O···H distance than the intermixed structure. In general, achieving chiral resolution in molecular systems has been a longstanding problem, with many potential applications, such as heterogeneous catalysis, nonlinear optics, and drug screening.[48–50] This difficulty arises because nature prefers chiral intermixing over separation during the growth of bulk crystals. It has been reported that even if molecules form an intermixed structure in bulk crystals, they can make phase-separation structures on the surface.[51,52] The reason for this difference in chiral growth behavior between surface and bulk is that there are interlayer interactions within the molecular crystals that differ from the molecule-surface interactions. Indenofluorene molecule is one of the rare examples that has structural data for both bulk and surface available in literature because Ozdemir *et al.* reported x-ray diffraction data and density functional theory calculation results for bulks and in this article we report our data obtained from STM on surfaces.[15]

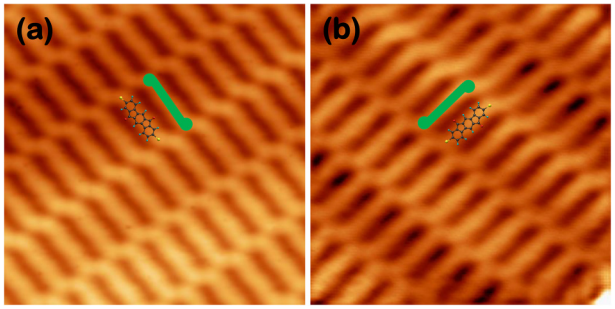

FIG. 5. STM images for two different prochiral DBIFD domains. (a) δ-DBIFD; (b) λ-DBIFD. (a) $I_T = 0.05$ nA, $V_S = -1.0$ V; (b) $I_T = 0.05$ nA, $V_S = -1.0$ V. The size of STM images: (a) and (b) 6.5 × 6.5 nm^2.

V. CONCLUSIONS

We studied the array structures of DBIFD molecules on Au(111) using STM and DFT calculations. DBIFD molecules formed monolayer molecular islands with strong shape anisotropy after annealing at temperatures higher than 200 K. Based on the observed STM images, we proposed an atomic model of an alternating-tread stair structure based on four O···H bonds and one Br···Br halogen bond per molecule, as supported by our DFT calculations. Our study shows that molecules can form phase-separated homoprochiral domains on the surface, although they prefer intermixed heteroprochiral domains in bulk layers; this has the potential to be applied to the chiral separation of organic molecules.

ACKNOWLEDGMENTS

The authors gratefully acknowledge financial support from the National Research Foundation of Korea (Grants Nos.

2021R1A2C1012526, 2021R111A1A01053172, and 2018R1A4A1024157) and Korea University grants. This work was supported by the Supercomputing Center/Korea Institute of Science and Technology Information with supercomputing resources and technical support (No. KSC-2014-C1-031).

DATA AVAILABILITY

The data that support the findings of this study are available within the article.

REFERENCES

[1]I. Kymissis, *Organic Field Effect Transistors: Theory, Fabrication and Characterization* (Springer Science, New York, 2009).
[2]R. J. Komp, *Practical Photovoltaics Electricity From Solar Cells* (Aatec Publications, Ann Arbor, MI, 2001).
[3]S. R. Forrest and M. E. Thompson, Chem. Rev. **107**, 923 (2007).
[4]H. Sirringhaus, Adv. Mater. **26**, 1319 (2014).
[5]J. E. Anthony, Chem. Rev. **106**, 5028 (2006).
[6]N. Koch, ChemPhysChem **8**, 1438 (2007).
[7]Z. Sun, Q. Ye, C. Chi, and J. Wu, Chem. Soc. Rev. **41**, 7857 (2012).
[8]A. Shimizu, S. Nobusue, H. Miyoshi, and Y. Tobe, Pure Appl. Chem. **86**, 517 (2014).
[9]Y. Tobe, Chem. Rec. **15**, 86 (2015).
[10]T. Kubo, Chem. Lett. **44**, 111 (2015).
[11]G. E. Rudebusch *et al.*, Nat. Chem. **8**, 753 (2016).
[12]S. Thomas and K. S. Kim, Phys. Chem. Chem. Phys. **16**, 24592 (2014).
[13]K. Fukuda, T. Nagami, J. Fujiyoshi, and M. Nakano, J. Phys. Chem. A **119**, 10620 (2015).
[14]T. Nakagawa, D. Kumaki, J. Nishida, S. Tokito, and Y. Yamashita, Chem. Mater. **20**, 2615 (2008).
[15]M. Ozdemir *et al.*, RSC Adv. **6**, 212 (2016).
[16]Z. Majzik, N. Pavli˘ek, M. Vilas-Varela, D. Pérez, N. Moll, E. Guitián, G. Meyer, D. Peña, and L. Gross, Nat. Commun. **9**, 1198 (2018).
[17]M. Di Giovannantonio *et al.*, J. Am. Chem. Soc. **140**, 3532 (2018).
[18]M. Di Giovannantonio *et al.*, J. Am. Chem. Soc. **141**, 12346 (2019).
[19]M. Di Giovannantonio, Q. Chen, J. I. Urgel, P. Ruffieux, C. A. Pignedoli, K. Müllen, A. Narita, and R. Fasel, J. Am. Chem. Soc. **142**, 12925 (2020).
[20]C. Martín-Fuentes *et al.*, Chem. Commun. **57**, 7545 (2021).
[21]G. Kresse and J. Hafner, Phys. Rev. B **47**, 558 (1993).
[22]G. Kresse and J. Hafner, Phys. Rev. B **49**, 14251 (1994).
[23]P. E. Blöchl, Phys. Rev. B **50**, 17953 (1994).
[24]J. P. Perdew, K. Burke, and M. Ernzerhof, Phys. Rev. Lett. **77**, 3865 (1996).
[25]S. Grimme, Comput. Chem. **25**, 1463 (2004).
[26]S. Grimme, Comput. Chem. **27**, 1787 (2006).
[27]O. Hassel, Science **170**, 497 (1970).
[28]P. Metrangolo, G. Resnati, and H. D. Arman, *Halogen Bonding: Fundamental and Applications* (Springer-Verlag, Berlin, 2008).
[29]G. R. Desiraju and R. Parthasarathy, J. Am. Chem. Soc. **111**, 8725 (1989).
[30]P. Metrangolo, F. Meyer, T. Pilati, G. Resnati, and G. Terraneo, Angew. Chem. Int. Ed. **47**, 6114 (2008).
[31]P. Metrangolo and G. Resnati, Science **321**, 918 (2008).
[32]C. B. Aakeröy, M. Fasulo, N. Schultheiss, J. Desper, and C. Moore, J. Am. Chem. Soc. **129**, 13772 (2007).
[33]H. Walch, R. Gutzler, T. Sirtl, G. Eder, and M. Lackinger, J. Phys. Chem. C **114**, 12604 (2010).
[34]J. K. Yoon, W.-J. Son, K.-H. Chung, H. Kim, S. Han, and S.-J. Kahng, J. Phys. Chem. C **115**, 2297 (2011).
[35]J. K. Yoon, W.-J. Son, H. Kim, K.-H. Chung, S. Han, and S.-J. Kahng, Nanotechnology **22**, 275705 (2011).
[36]J. C. Russell, M. O. Blunt, J. M. Garfitt, D. J. Scurr, M. Alexander, N. R. Champness, and P. H. Beton, J. Am. Chem. Soc. **133**, 4220 (2011).
[37]R. Gutzler, O. Ivasenko, Ch. Fu, J. L. Brusso, F. Rosei, and D. F. Perepichka, Chem. Commun. **47**, 9453 (2011).
[38]K.-H. Chung, J. Park, K. Y. Kim, J. K. Yoon, H. Kim, S. Han, and S.-J. Kahng, Chem. Commun. **47**, 11492 (2011).
[39]S.-K. Noh, J. H. Jeon, W. J. Jang, H. Kim, S.-H. Lee, M. W. Lee, J. Lee, S. Han, and S.-J. Kahng, Chem. Phys. Chem. **14**, 1177 (2013).
[40]S. Yasuda, A. Furuyaa, and K. Murakoshi, RSC Adv. **4**, 58567 (2014).
[41]W.-J. Jang, K. H. Chung, M. W. Lee, H. Kim, S. J. Lee, and S.-J. Kahng, Appl. Surf. Sci. **309**, 74 (2014).
[42]U. S. Jeon, M. H. Chang, W.-J. Jang, S.-H. Lee, S. Han, and S.-J. Kahng, Appl. Surf. Sci. **432**, 332 (2018).
[43]M. H. Chang, W.-J. Jang, M. W. Lee, U. S. Jeon, S. Han, and S.-J. Kahng, Appl. Surf. Sci. **432**, 110 (2018).
[44]Y. Kikkawa, M. Nagasaki, E. Koyama, S. Tsuzuki, and K. Hiratani, Chem. Commun. **55**, 3955 (2019).
[45]J. Lawrence, G. C. Sosso, L. Đorđević, H. Pinfold, D. Bonifazi, and G. Costantini, Nat. Commun. **11**, 2103 (2020).
[46]R. S. Rowland and R. Taylor, J. Phys. Chem. **100**, 7384 (1996).
[47]J. Tschakert *et al.*, Nat. Commun. **11**, 5630 (2020).
[48]Y. Wang, N. S. Hush, and J. R. Reimers, Phys. Rev. B **75**, 233416 (2007).
[49]D. B. Amabilino, *Chirality at the Nanoscale Nanoparticles, Surfaces, Materials and More* (Wiley-VCH, Weinheim, 2009).
[50]K.-H. Ernst, Top. Curr. Chem. **265**, 209 (2006).
[51]J. Weckesser *et al.*, Phys. Rev. Lett. **87**, 096101 (2001).
[52]Q. Chen *et al.*, Langmuir **18**, 3219 (2002).